Supplementary materials

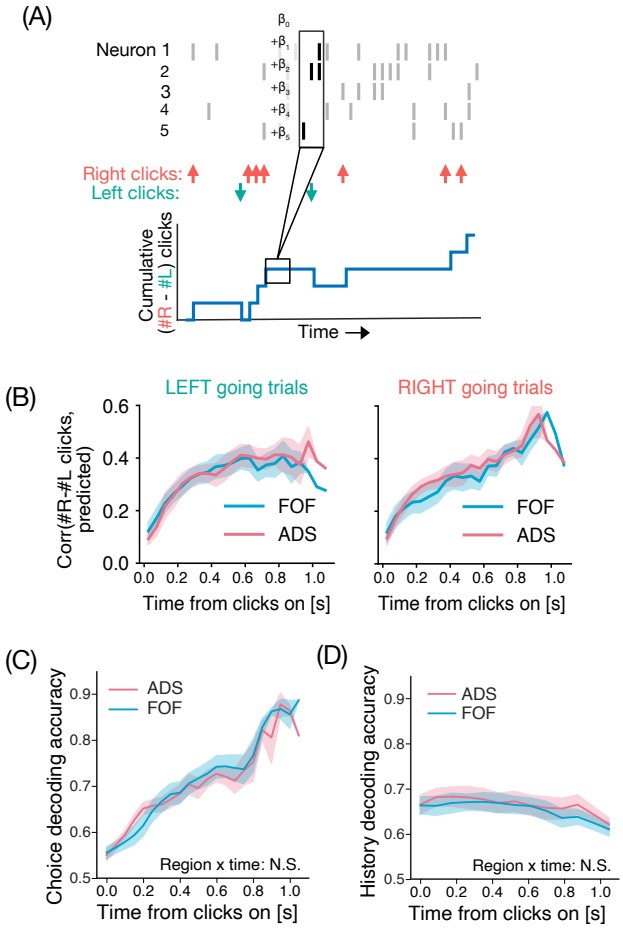

Supplementary Figure 1 **Similar strength and timecourse of stimulus, choice and history decoding in FOF and ADS (A)** Schematic showing the linear decoder designed to predict the cumulative click difference in the number of right and left clicks at any given time during a trial using a linear combination of neural activity from FOF or ADS. We assumed a neural encoding lag of 100ms and regularized the linear weights on neurons with L1 penalty using cross-validation. **(B)** Stimulus decoding performance (mean $\pm$ sem) of the linear decoder on held-out time points as a function of time from stimulus onset (n = 12 sessions) performed separately for left (left panel) and right (right panel) going trials to control for choice. The two areas show high decoding performance which evolves with a similar timecourse (P$>$ 0.05, two-way RM ANOVA). **(C)** Cross-validated choice decoding accuracy as a function of time from stimulus onset for FOF (aqua blue) and ADS (pink) neural activity (n = 12 sessions). Time courses and strength of choice decoding from the two populations did not differ significantly (P$>$ 0.05 two-way RM ANOVA). Decoding was performed with an L2 regularized logistic decoder, while controlling for number of neurons from the two areas. **(D)** Same as C but decoding for choice from past trial (n = 12 sessions). No significant differences were observed between the two populations (P $>$ 0.05, two-way RM ANOVA)

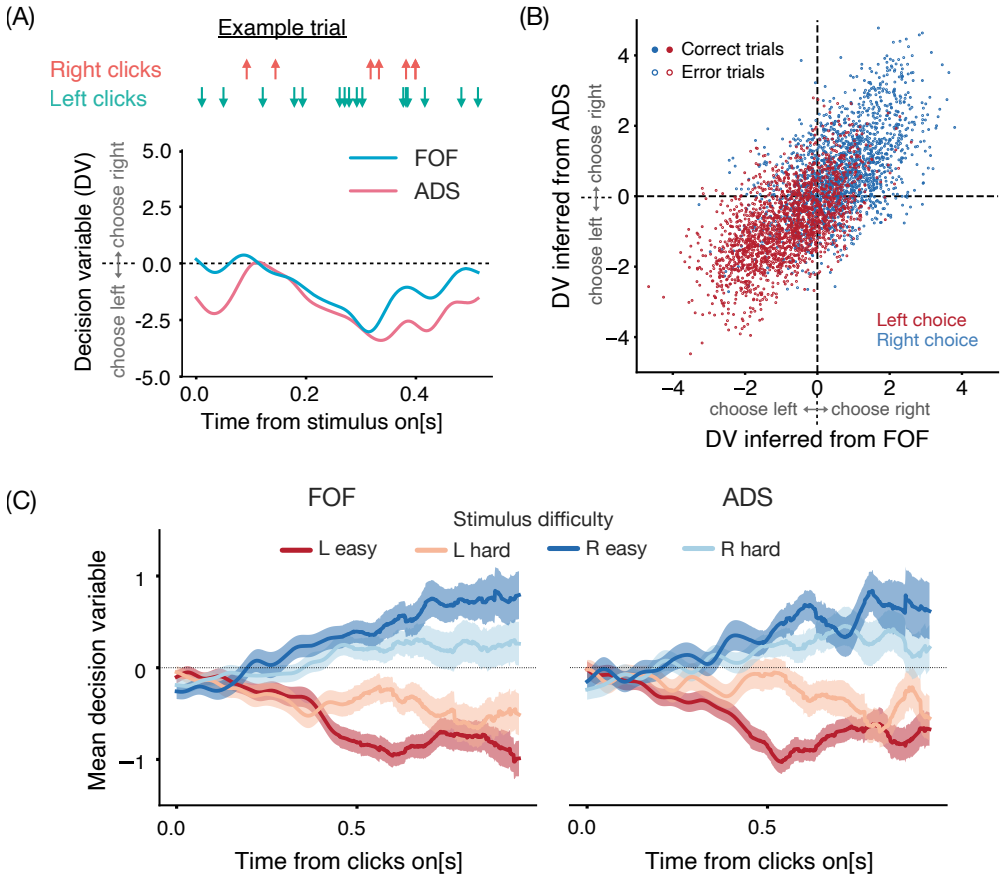

Supplementary Figure 2 **Decoding decision variable from FOF and ADS population activity (A)** Example trial showing the trajectory of the decision variable (DV) decoded from the simultaneous population activity of FOF and ADS (blue, pink line respectively), using the logistic decoder (see Methods). The DV represents the log odds ratio of making one choice over another, with higher positive (negative) values indicating a stronger likelihood of rightward (leftward) choices. Both regions have comparable DV time-courses, and seem to be influenced by the sequence of right and left clicks (coral, green arrows respectively). **(B)** Scatter plot comparing DV values inferred from FOF (x-axis) and ADS (y-axis) activity at the same time-points from an example session. Dots represent time-points across trials, with filled (unfilled) circles indicating correct (incorrect) trials. Points are color-coded according to the actual choice of the animal, with blue (red) indicating rightward (leftward) choices. The DV inferred from both areas shows good correspondence with each other and the true choice. **(C)** Mean DV trajectories from FOF (left) and ADS (right) over time from an example session and separated by stimulus difficulty (red - easy leftward stimulus, light red - hard leftward, blue - easy rightward, light blue - hard rightward). Shaded regions indicate S.E.M. Both regions show similar DV time-courses and similar dependence on stimulus difficulty.

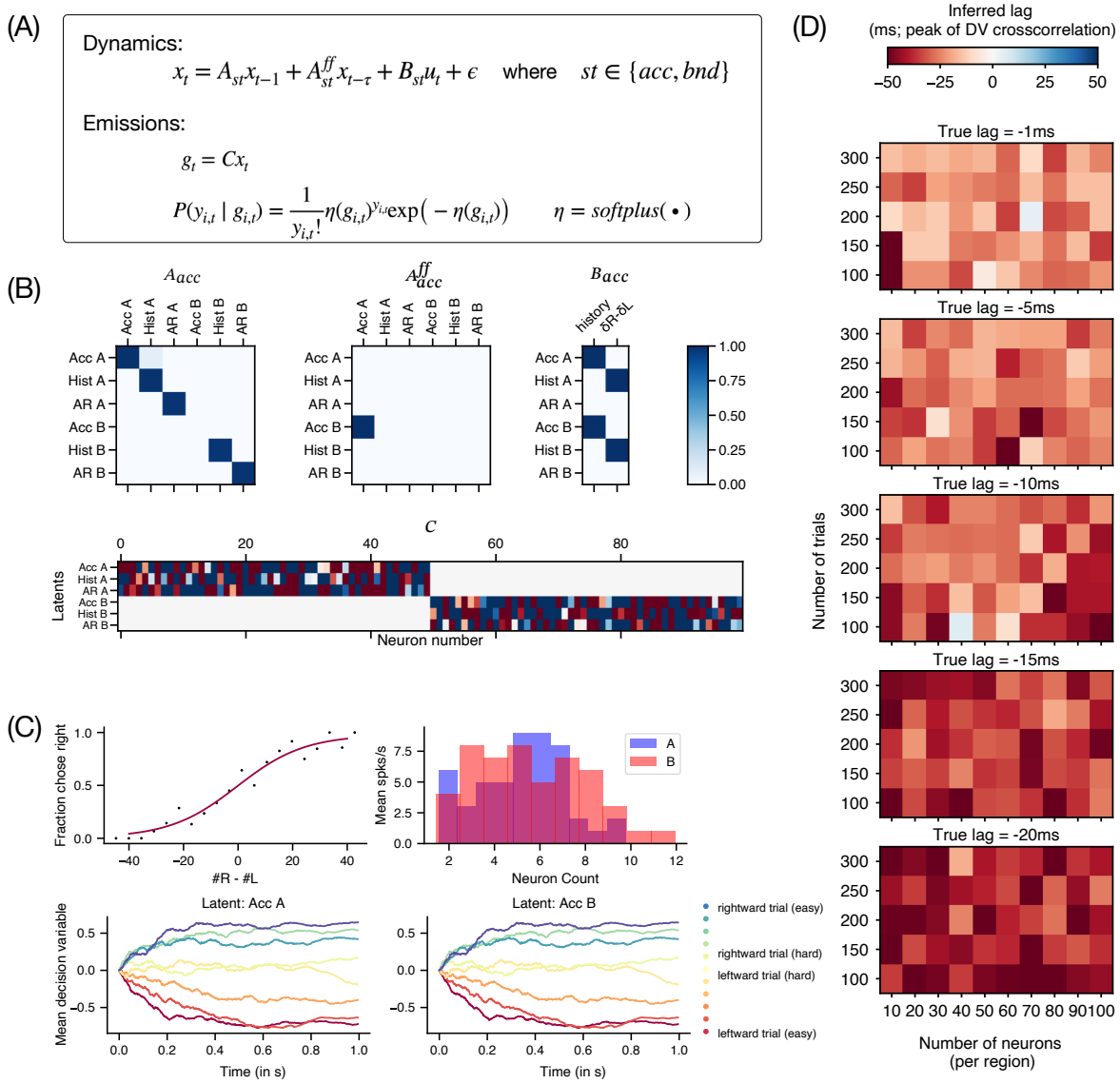

Supplementary Figure 3 **Simulations used to validate the decision variable cross-correlation analysis.** **(A)** Equations used to simulate two regions with feedforward flow of accumulator dynamics. (Top) The low-dimensional latents in the two regions x_t represent accumulator variables (Acc), history (Hist) and autoregressive (AR) terms that evolve according to linear dynamics with dynamics A_{st} that are different during accumulation ($st = acc$) and bound-hitting ($st = bnd$). During accumulation, one region's accumulator dynamics (region B) are influenced by feed-forward inputs from the other region's accumulator (region A) according to A^{ff}_{acc} with delay τ. Both regions receive external inputs u_t (including stimulus clicks and history) according to B_{st} and Gaussian noise ϵ. (Bottom) The mean firing rates g_t of neurons in the two regions reflect a high-dimensional projection C of the aforementioned latents x_t. These are then transformed through a softplus function (to enforce positive firing rates) into Poisson distributed spikes y_t. **(B)** (Top) Schematized A_{acc}, A^{ff}_{acc} and B_acc (Bottom) Linear weights C that transform latents (y-axis) into mean firing rates of individual neurons (x-axis). **(C)** (Top left) Fraction chose right based on thresholded values of the accumulator, showing a monotonic dependence on the stimulus. (Top right) Firing rate distributions in the two regions showing substantial heterogeneity and overlap. (Bottom) Mean decision variables across trials of the same stimulus difficulty for the two accumulator latents, showing a separation by difficulty. **(D)** (Top to bottom) Inferred lag measured by the peak of the decision-variable cross-correlation, for increasing true lags between the regions as a function of number of neurons (x-axis) and trials (y-axis). Even though the exact value of lag is not recovered for low trial and/or neuron counts, the direction of flow can be accurately inferred. Increasing color intensities show that the measured peak lag is sensitive to the true lag values.

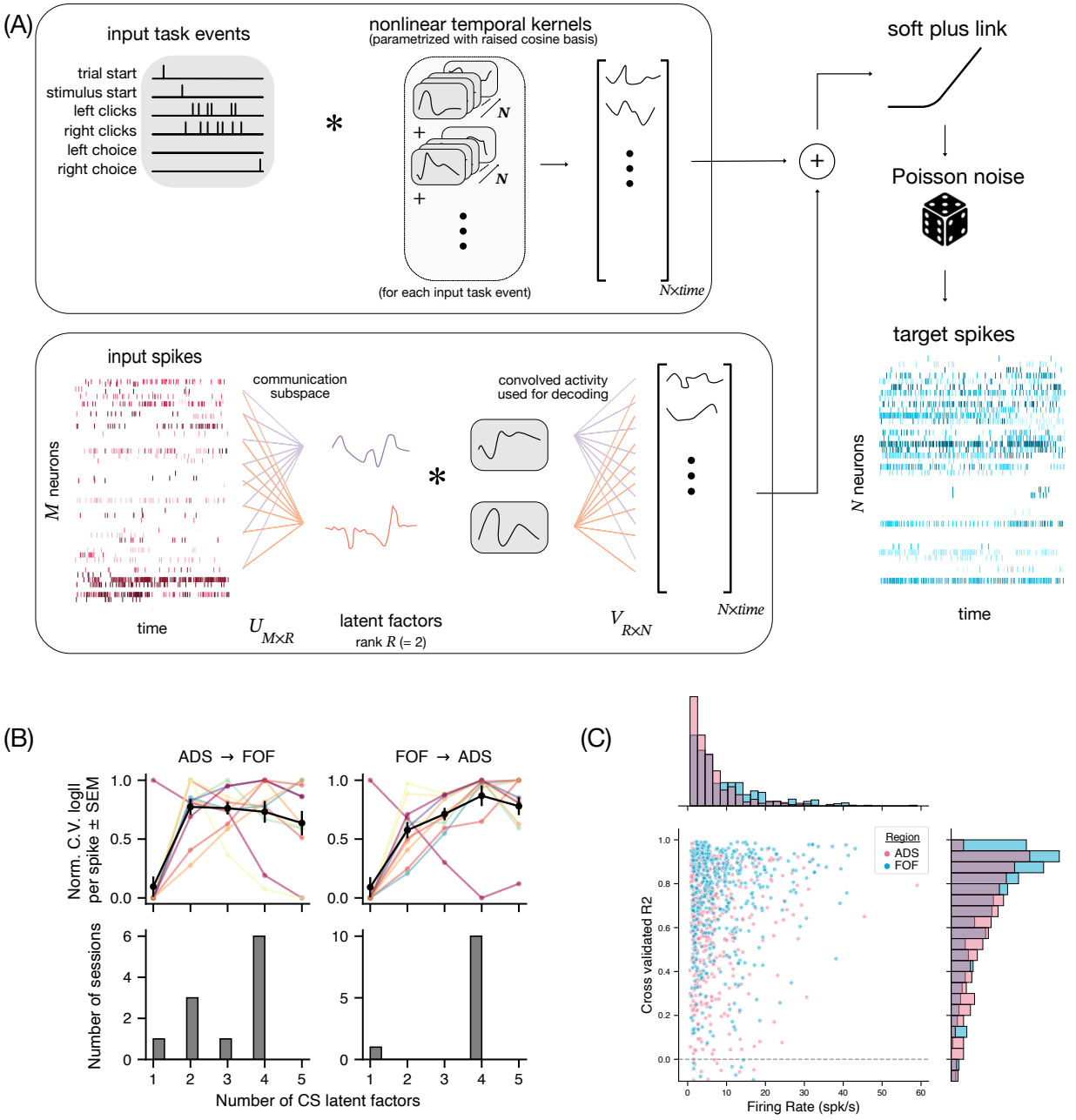

Supplementary Figure 4 **Reduced rank GLM captures the low-dimensional communication subspace between FOF and ADS (A)** Schematic of the reduced rank GLM approach. The target variables are sequences of spikes for each of N neurons in the output region (blue rasters), which are modelled as a generalized linear model with a soft plus link function and poisson noise distribution. The predictors consist of task events (top box, left panel) and sequences of spikes from M neurons in the input region (bottom box, red rasters). Task events are convolved with nonlinear temporal kernels parameterized with raised cosine bases - one per task event per output neuron - allowing them to have temporally extended effects (top box, grey boxes). Spikes from the M neurons in input region are first projected into a reduced R-dimensional communication subspace using learnt weights $U_{M\times R}$, yielding a small number of latent factors (bottom box, colored curves). These latent factors are then convolved with temporal kernels (grey boxes) and influence the N neurons in the output region through learnt output weights $V_{R\times N}$. **(B)** Required dimensionality of the communication subspace. (Top) Normalised cross-validated log likelihood per spike, as a function of the dimensionality of the communication subspace. Colored curves individual sessions, black represents mean across sessions. (Bottom) Distribution of the optimal dimensionality of the communication subspace across sessions. (Caption continued on next page).

Supplementary Figure 4 (Continued from previous page) Based on both these measures, the smallest dimension required (≤ 4) was used for each session, with most sessions warranting a 4-dimensional communication subspace. **(C)** Cross validated r-squared values across sessions of the reduced rank GLM (ADS = 0.64 $\pm$ 0.01, FOF = 0.73 $\pm$ 0.01 mean $\pm$ sem), plotted as a function of the session average firing rates - colors represent different directions of communication, with ADS (pink) or FOF (blue) as output regions. In ADS (FOF), 0.12 (0.09) fraction of cells had R2 < 0. These cells were excluded while computing the mean R2.

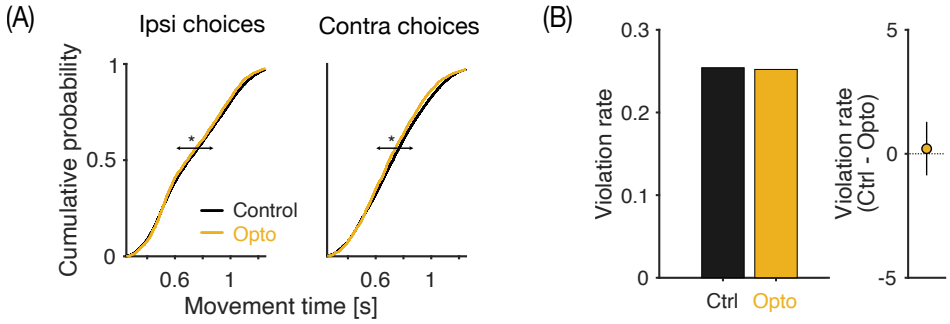

Supplementary Figure 5 **Silencing FOF axon terminals in ADS: effect on movement (A)** Silencing reduces movement times. Cumulative distribution of movement times across (n = 6) rats on control (black) and whole-trial inactivation (orange) trials. Movement time is defined as the time taken by the rats to leave the center port and enter one of the two side ports to report their choice. Silencing of FOF axon terminals in ADS significantly reduced the mean movement times for both choices ipsiversive (left, P = 0.05 Mann-Whitney U test) and contraversive (right, P = 0.001 Mann-Whitney U test) to the laser. **(B)** Silencing doesn't affect rate of trial completion (left) Mean violation rates observed across rats (n=6) on control (black) and whole-trial inactivation (orange) trials. Rats are expected to "fixate" at the center port for 1.5s from trial initiation, failure to do so aborts the trial. Violation rates measure the rate of premature exits from the center port. An increased violation rate might reflect an inability to complete trials due to gross motor/cognitive impairment induced by laser. (right) Mean violation rates between control and opto trial were not different (P = 0.58, non-parametric bootstrap test).

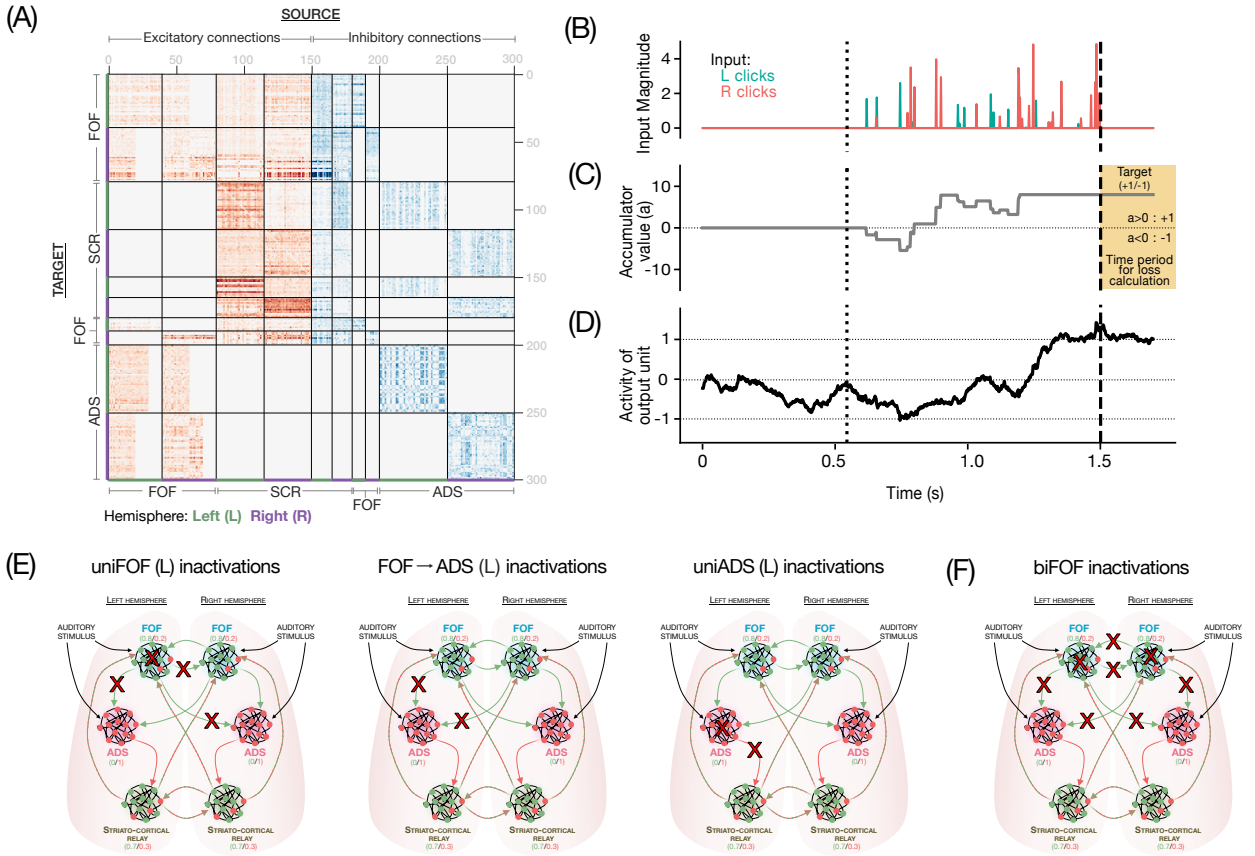

Supplementary Figure 6 **Training details of multi-region recurrent neural network model (A)**: Connectivity diagram of recurrent neural network, showing modular structure and following Dale's law. Excitatory connections are shown in red, and inhibitory in blue, with lines demarcating individual modules in a hemisphere. **(B)**: Example trace of stimulus inputs to the network, showing leftward and rightward clicks with variable timing and magnitudes. **(C)**: Accumulator value computed from stimulus trace above[32]. The final thresholded accumulator value acts as the training target for network outputs on this trial. **(D)**: Example activity of a network output unit that has successfully matched the target output on this trial. **(E)**: Schematics showing all activity and projections that were silenced in unilateral inactivation experiments during training. (Left to Right): unilateral FOF inactivations, FOF → ADS inactivations, unilateral ADS inactivations. Red crosses indicate inactivated elements. **F**: Same as E, but for bilateral FOF inactivations.

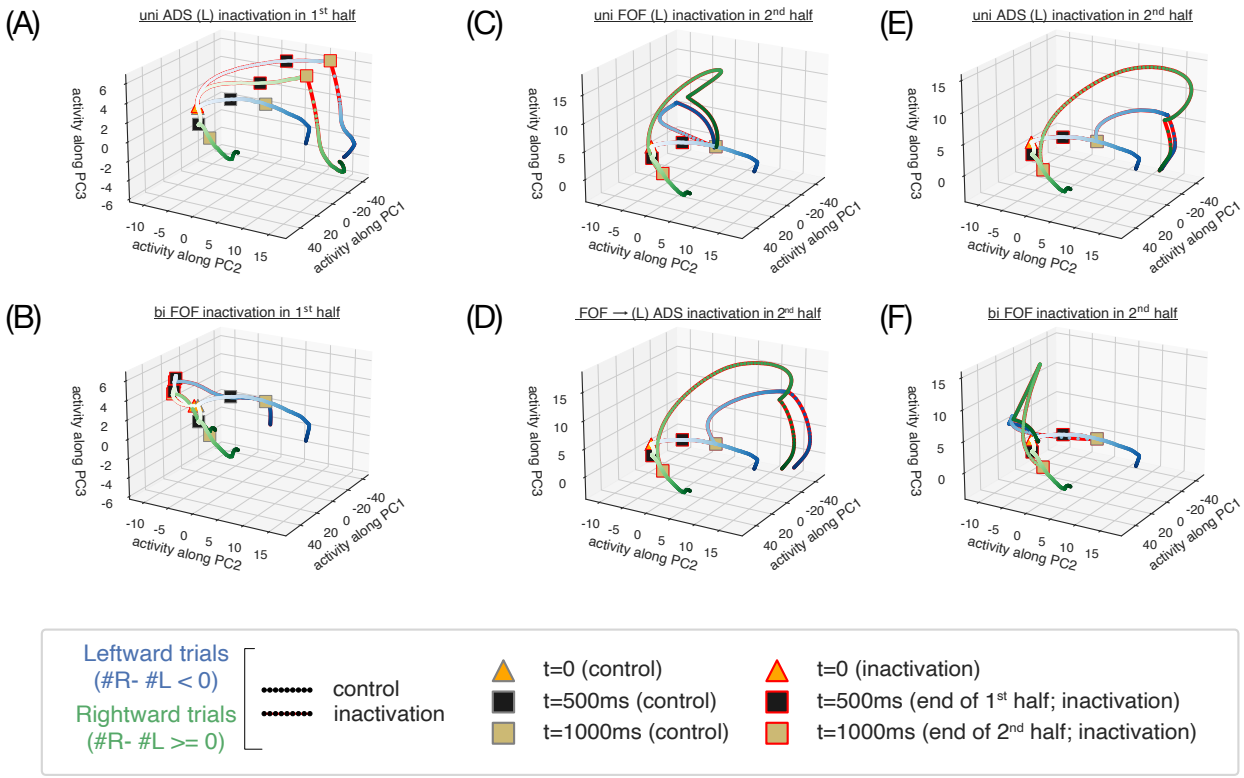

Supplementary Figure 7 **Network dynamics during 1st and 2nd half inactivations** Projections of network activity onto first 3 principal components showing trajectories on rightward (green) and leftward (blue) trials. Red edges represent inactivation trials, and black/yellow boxes represent end of 1st/2nd half respectively. Unilateral inactivation of ADS in the 1st half (A) leads to rightwards trajectories diverging from control and incorrectly driving leftward choices, while bilateral inactivation of FOF in the 1st half (B) recovers towards correct choices subsequently. Unilateral inactivation of all regions in the second half (FOF (C), FOF→ADS projections (D), ADS (E) or bilateral inactivations of FOF (F)) drives incorrect choices and shows no recovery.

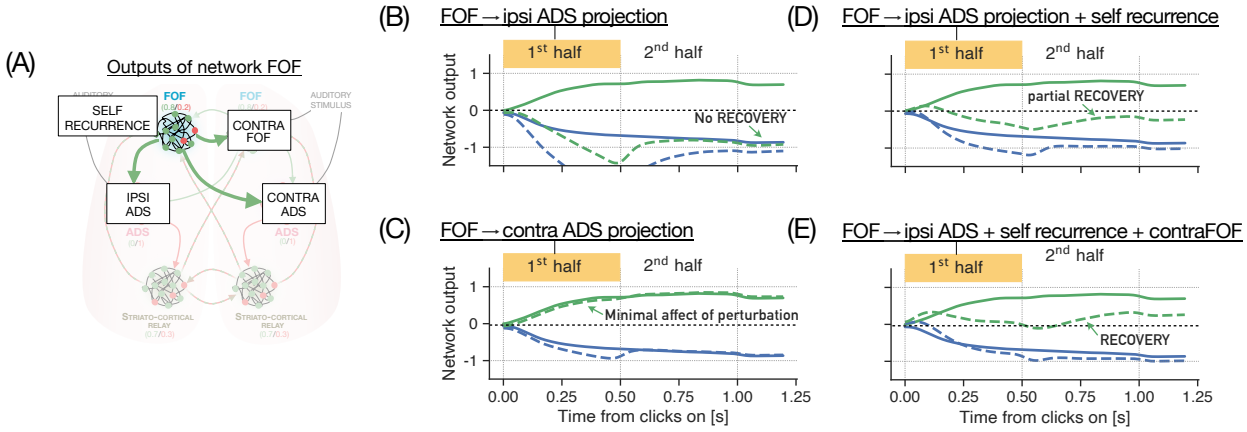

Supplementary Figure 8 **Network outputs in response to in-silico perturbations (A)** Schematic of model FOF output projections from a single hemisphere, targeted for in-silico perturbations in the 1st half. Perturbations of left FOF's projections to ipsilateral ADS (**B**) led to network outputs diverging from control on rightward inactivation trials (dotted green) with no recovery, while perturbations of the projections to contralateral ADS (**C**) had no inactivation effect to begin with - suggesting that the ipsilateral ADS projections were largely responsible for inactivation effects. Additionally perturbing the self recurrence projection (**D**) or the contralateral FOF projection (not shown) invites partial recovery, while perturbing both (**E**) invites nearly complete recovery, with outputs crossing the decision threshold (y=0 line).